J Appl Electrochem (2013) 43:1069–1078
DOI 10.1007/s10800-013-0567-9

ORIGINAL PAPER

Design of a reference electrode for high-temperature PEM fuel cells

Sebastian Kaserer · Christoph Rakousky · Julia Melke · Christina Roth

Received: 29 January 2013 / Accepted: 17 May 2013 / Published online: 28 May 2013

Abstract In this work, we present the design of an external reference electrode for high-temperature PEM fuel cells. The connection between the reference electrode with one of the fuel cell electrodes is realized by an ionic connector. Using the same material for the ionic connection as for the fuel cell membrane gives us the advantage to reach temperatures above 100 °C without destroying the reference electrode. This configuration allows for the separation of the anode and cathode overpotential in a working fuel cell system. In addition to the electrode overpotentials in normal hydrogen/air operation, the influence of CO and CO + H_2O in the anode feed on the fuel cell potentials was investigated. When CO poisons the anode catalyst, not only the anode potential increased, but also the cathode overpotential, due to fewer protons reaching the cathode. By the use of synthetic reformate containing hydrogen, carbon monoxide and water on the anode, fuel cell voltage oscillations were observed at high constant current densities. The reference electrode measurements showed that the fuel cell oscillations were only related to reactions on the anode side influencing the anode overpotential. The cathode potential, in contrast, was only negligibly affected by the oscillations under the applied conditions.

Keywords HT-PEM fuel cell · Reference electrode · CO poisoning · Electrode overpotential · Oscillations

S. Kaserer · C. Roth (✉)
Renewable Energies Group, Institute for Materials Science, Technische Universität Darmstadt, Petersenstr. 23, 64287 Darmstadt, Germany
e-mail: christina.roth@fu-berlin.de

C. Rakousky
Institute of Energy and Climate Research, Institute for Energy Research, Forschungszentrum Jülich GmbH, 52425 Jülich, Germany

J. Melke
Institute for Applied Materials, Karlsruher Institute of Technology, 76344 Eggenstein-Leopoldshafen, Germany

C. Roth
Institute of Chemistry and Biochemistry, Physical and Theoretical Chemistry, Freie Universität Berlin, 14195 Berlin, Germany

1 Introduction

The phosphoric acid fuel cell (PAFC) is one of the oldest types of fuel cells, which was used in different application fields like transit buses [1, 2], power plants (~200 kW) [1–3] and noise-free lightweight electric power generators (~5 kW) [1] which are at the end of their testing phase or already commercialized. With the application of polybenzimidazole (PBI) membranes as proton conductive separator between anode and cathode in the mid-1990s [4, 5], the interest in PAFC systems soared again. With this PBI material, the high-temperature polymer electrolyte membrane fuel cell (HT-PEMFC) with phosphoric acid as electrolyte was developed. One of the advantages of this kind of fuel cells is their enhanced tolerance against carbon monoxide (CO) poisoning. With working temperatures between 160 and 200 °C, amounts of about 1–3 % CO in the anode fuel can be tolerated [6–8]. This advantage makes HT-PEMFCs perfectly suitable for steam reformed hydrogen from petroleum gas and other fossil or biofuels. The combination of reformer and fuel cell next to each other offers the advantage that hydrogen storage is not necessary for such systems. Moreover, the waste heat of the fuel cell can be used further enhancing the overall

performance of the system (combined heat and power systems) [3, 8]. Due to the fact, that steam reformers do not produce pure hydrogen, but hydrogen with different amounts of CO, CO_2, water and several other impurities, depending on the feed gas [9, 10], higher fuel cell temperatures are needed. A representative gas mixture from a copper catalyst-based methanol reformer (280 °C, steam to methanol ratio 1.5 and pressure 3 bar) is ~65 mol % H_2, ~20 mol % CO_2, ~12.5 mol % H_2O and ~2.5 mol % CO [9]. But although the higher temperature reduces the poisoning effects of CO on the platinum catalyst, it still adsorbs on its surface and blocks free adsorption sites resulting in an increase in the anode overpotential.

Beyond the CO adsorption on the anode side, also phosphoric acid (H_3PO_4) adsorption on the cathode side might be an issue. Previous investigations like cyclic voltammetry studies [11–13], FT-IR spectroscopy measurements [12, 14, 15], quartz crystal microbalance [16] and X-ray absorption experiments [13, 17] showed that the phosphoric acid adsorption on platinum surfaces is potential dependent. By blocking the electrochemically active surface, the ORR (oxygen reduction reaction) is negatively affected.

Due to the fact that both adsorption processes have an effect on the electrode potentials (CO poisoning) or are potential dependent (H_3PO_4 adsorption), it is desirable to know the exact potentials at the anode and cathode side. With this information, the poisoning effect of strongly adsorbed ions and molecules can be explained. To measure anode and cathode potential separately, it is necessary to integrate a reference electrode with a known constant potential in the fuel cell assembly. In recent literature, different options for a suitable reference electrode setup, like sandwich type [18, 19] and edge type [20–24], were described. Unfortunately, such reference electrode assemblies have different drawbacks. When the reference electrode is positioned on the edge of the membrane, the measured potential is often dominated by the electrode in closer proximity due to slight misalignment of the electrodes [21, 25, 26]. Internal reference electrodes in contrast have the disadvantage that the charge transport in the membrane is perturbed by the presence of the electrode and its trailing wires [22]. To avoid these disadvantages, an alternative setup was used as invented by Hinds et al. [27]. Their reference electrodes were connected to the fuel cell electrode using small Nafion tubes as ionic connectors. These "salt bridges" were inserted through holes drilled through the end plates of a low-temperature PEM fuel cell. By adapting this principle to high-temperature PEM fuel cells, we were able to measure the different electrode potentials with respect to the fuel cell voltage.

2 Experimental

2.1 Fuel cell testbench and reference electrode assembly

For all fuel cell investigations, a single cell HT-PEM fuel cell with 25 cm^2 cell area was used. The fuel cell assembly consisted of graphite flow fields and alumina end plates enclosing the heaters. The MEAs were supplied by Fumatech GmbH (Germany) and Advent Energy Technologies S.A. (Greece). Both producers used chemically modified PBI membranes between two gas diffusion electrodes (GDE) consisting of a graphite felt/paper and a catalyst layer of carbon supported platinum nanoparticles. Due to confidentiality reasons, no information on the catalyst specifics and the MEA preparation process can be disclosed.

All fuel cell measurements were obtained with a homemade fuel cell testbench. For the gas flow regulation of hydrogen, nitrogen and oxygen, three Alicat Scientific mass flow controllers with a maximum flow of 500 ml/min (H_2 and N_2) and 200 ml/min (O_2) were used. To provide synthetic air on the cathode, the oxygen and nitrogen tubes were connected. For measurements with carbon monoxide, an additional mass flow controller (Bronkhorst, max. 5 ml/min) was connected to the fuel cell anode inlet. To control the fuel cell temperature, two thermo couples (type K) and two heating elements (200 W) were connected to the fuel cell flow fields and each controlled by a Jumo iTRON 32 temperature controller. The electrical load (ITS, 724X/7241-Z) measuring the voltage and current of the fuel cell as well as the mass flow controllers were connected to a laptop and operated with an in-house programmed LabView program.

To measure the anode and cathode potentials independently from each other, it was necessary to modify the fuel cell assembly. By drilling a small hole into the flow field and the GDE, it was possible to insert a small PFA tube (inner diameter 0.85 mm) filled with PBI + H_3PO_4 (doping level ~35 H_3PO_4 molecules per repeating unit of PBI) membrane material into the fuel cell. To prevent a gas leak on this side, the tube was sealed with high-temperature resisting silicon glue (Wekem GmbH, WK-138-200). The other end of the tube was connected to a glass container filled with concentrated phosphoric acid (85 % orthophosphoric acid for analysis, Merck KGaA). As external reference electrode, an Ag/AgCl (Schott Instruments, Scienceline B3420+) electrode was placed into this chamber. With this ion bridge assembly, an ionic link between the membrane surface and the external reference electrode was achieved. The schematic diagram of the fuel cell // ion bridge // external reference electrode is shown in Fig. 1. A photograph of the used single cell with the inserted ion bridge is provided in Fig. 2.

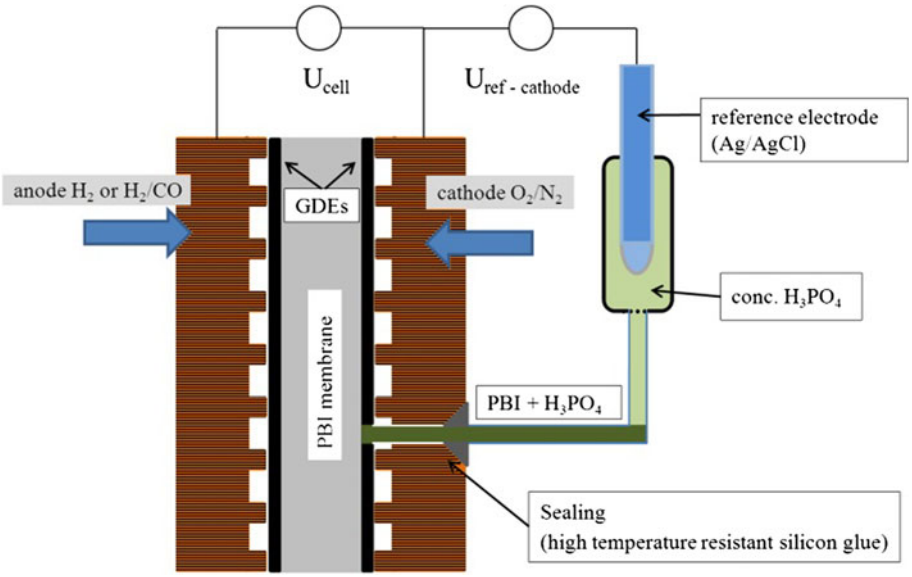

Fig. 1 Modified through-plate configuration for HT-PEM fuel cells with external reference electrode

All measurements were carried out at 160 °C. At the cathode, a 1:4 mixture of oxygen and nitrogen gas was used. The gas composition of the anode changed with the different experiments. To avoid effects related to starvation on the overpotentials [28], an excess amount of fuel gas compared to the maximum current density was provided for each measurement. The exact ratio between the introduced gas and consumed gas (λ_{H_2} and λ_{air}) for the different measurements is given in the Results and Discussion section. The gas outlets were opened to the atmosphere. To obtain the anode and cathode potential under poison-free conditions, pure hydrogen was fed into the cell during these experiments. The variation of the overpotentials with CO as catalyst poison was investigated with different concentrations of CO and CO + H_2O in the anode gas. The hydrogen was humidified by passing through a heated bubbler. The mentioned amount of additional water in the cell was calculated with the gas flow entering the humidifier under the assumption of 100 % relative humidity. To prevent water condensation between the bubbler and the fuel cell, the connecting tube was heated to temperatures above the humidifier temperature.

By giving an absolute value of anode humidification, we have to take into account that beyond the water from the humidifier also H_2O, which is produced at the cathode, can diffuse through the membrane and enter the anode. The amount of water from the cathode therefore depends on the membrane type, the cell temperature and the steam partial pressure difference between anode and cathode [29], which is strongly influenced by the current density and the produced water. The humidification level of the anode mentioned in the Sect. 3 refers to the calculated amount of water from the temperature-controlled bubbler only. A description of the anode humidification considering the additional water diffusion from the cathode side was not possible. Assuming that the steam partial pressure produced by the humidifier on the anode side is as high as that on the cathode, only small amounts of water diffuse through the PBI membrane. Therefore, the real amount of water at the anode could be slightly higher than reported.

2.2 Reference electrode data processing

The measured cell voltage (U_{cell}) at different current densities (i) is depending on several factors as mentioned in (2.1).

$$U_{\text{cell}} = U_0 - iR - \eta_A - \eta_C - \eta_d \tag{2.1}$$

$$U_0 = \Phi_C - \Phi_A(i = 0) \tag{2.2}$$

U_0 open circuit voltage; R resistance (membrane, current collectors, cable, etc.); $\eta_{A,C}$ anode and cathode activation overpotential; η_d diffusion overpotential; $\Phi_{A,C}$ anode, cathode potential.

To determine the activation overpotential ($\eta_{A,C}$), only the region where the diffusion (or mass transport) overpotential has a negligible influence ($\eta_d < \eta_{A,C}$; $\eta_d < iR$) on the i–V curve was investigated. For all measurements, the reference electrode was connected to the cathode side of the fuel cell. All results were corrected by the value of the constant reference electrode potential ($\Phi_{ref} \approx 270$ mV), by measuring the voltage between the reference electrode and the anode (Φ_A) at U_0 (open circuit voltage, $i = 0$). At U_0, the fuel cell anode acts as a reversible hydrogen electrode with a potential of approximately 0 mV.

The fact that the reference electrode is in contact with the fuel cell cathode makes it possible to measure the cathode potential (Φ_C) directly between the cathode and the reference electrode (Φ_{ref}). The cathode overpotential (η_C)

calculation is described in Eq. (2.3). The voltage measured between the reference electrode and the anode ($U_{ref\text{-}A}$) leads to the anode overpotential/potential (η_A/Φ_A) as described by (2.4).

$$\eta_C = U_0 - \Phi_C = U_0 - (U_{C-\mathrm{ref}} + \Phi_{\mathrm{ref}}) \quad (2.3)$$

$$\eta_A = \Phi_{\mathrm{ref}} - (U_{\mathrm{ref}-A} + iR) = \Phi_A \quad (2.4)$$

To obtain the true anode overpotential, Eq. (2.4) has to be corrected by the *iR* drop term. The resistance (R) was estimated under the assumption that the anode potential does not increase with the current density, due to the fast hydrogen oxidation reaction. Thus, the measured anode potential slope over current density in the ohmic region has its origin almost exclusively in the resistance. Due to this correction, the existing anode overpotential related to the hydrogen oxidation reaction, which is assumed to be quite small, is neglected. Therefore, an error of 10 % in the resistance is assumed. In this work, only the influence of CO poisoning on the anode overpotential is investigated. A correction based on the total membrane resistance tested with other techniques like impedance spectroscopy or the current interrupt method was not possible, because the contact area between the ion bridge and the membrane could not be determined exactly.

3 Results and discussion

3.1 Hydrogen/air operation

Representative *Φ-i* characteristics of a HT-PEM fuel cell at 160 °C are shown in Fig. 3. In this experiment, $\lambda_{H_2} = 1.2$ and $\lambda_{air} = 2.0$, respectively, were adjusted to the maximum current density ($\sim$0.55 A/cm^2). With this amount of fuel, starvation effects [28] on the electrode potentials can be neglected. The estimated resistance for the anode iR correction was 16.4 ± 2 mΩ. Conclusions as to the different anode and cathode activation overpotentials can be drawn up to current densities of around 0.5 A/cm^2 (0.1 V cell voltage). Beyond that point, the influence of the diffusion overpotential from the cathode and/or the anode becomes dominating over the other loss mechanisms, which is indicated by a kink in the i–V curve at this point. Analyzing the Tafel slope of the cathode overpotential showed a decrease of approximately 82 mV/dec, which closely fits the theoretical value of 2.303*RT/F* (86 mV/dec at 160 °C) [8]. The error between the measured Tafel slope and the literature value is about 5 %. This mismatch can have different reasons like the influence of the phosphoric acid + PBI electrolyte on the catalyst or a nonlinear heat distribution in the fuel cell. We have to accept the fact that a fuel cell environment will never provide conditions similar to laboratory half-cell experiments.

Between 0.9 and 0.1 V cell voltage, the cathode potential changes only by $\eta_C \approx 0.4$ V, before the mass transport overpotential is reached. According to this, the cathode potential in this region was between 0.9 and 0.5 V. The potential region, where phosphoric acid anions or similar molecules adsorb on Pt surfaces, is not clearly described for the HT-PEM environment in literature, since most studies were carried out under laboratory conditions at room temperature and in low concentrated phosphoric acid. However, all of these studies report a potential-dependent adsorption in the region of 0.1–0.9 V with a coverage maximum between 0.6 and 0.8 V [14, 17]. Hence, we have to assume that massive phosphoric acid coverage occurs on the cathode catalyst over the whole i–V curve. The abrupt anode overpotential increase in the region between 0 and 0.1 A/cm^2 is due to the applied iR correction procedure. But under the estimation that the anode potential does not exceed 0.1 V in this environment,

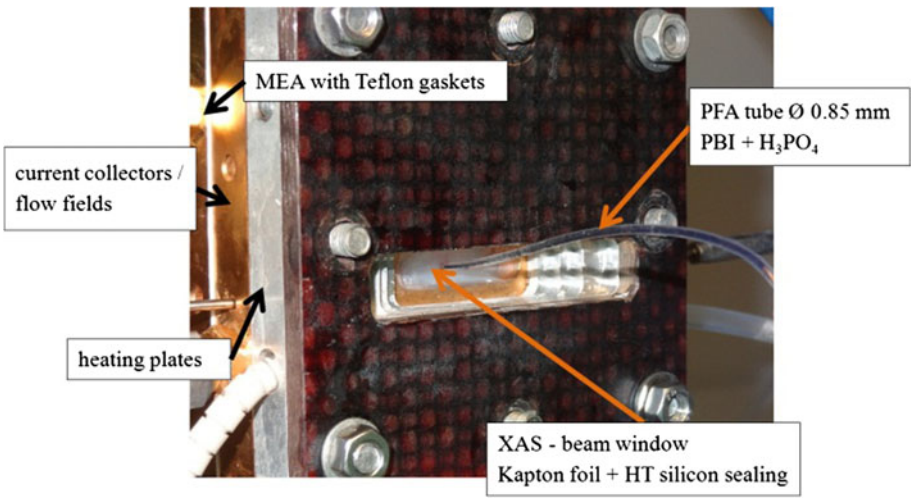

Fig. 2 Photograph of the HT-PEM single cell with inserted ionic connector

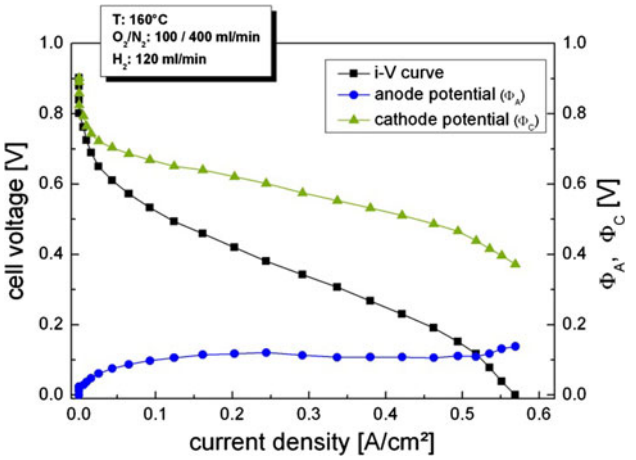

Fig. 3 Overview of the cell voltage, anode and cathode potential over current density. The resistance losses are not indicated in this graph. At current densities > 0.5 A/cm^2, the influence of η_d starts to dominate the other losses

H_3PO_4 as adsorbing anode catalyst poison does not seem to have a major influence on the fuel cell performance.

3.2 Hydrogen + CO/air operation

To investigate the influence of different amounts of CO in the anode fuel on the anode overpotential, i–V curves with up to 5.6 % carbon monoxide mixed with hydrogen were obtained. The fuel cell temperature for these measurements was 160 °C. The cathode gas mixture O_2:N_2 was 60:240 ml/min, while the hydrogen flow was 80 ml/min. To obtain different CO concentrations in the anode feed, different amounts of CO (0–4.8 ml/min) were mixed to the anode flow. The results of these measurements are shown in Fig. 4a (i–V curve) and b (power density curve). The more CO is added to the fuel, the more the maximum current density decreases. The reduction in the maximum power density is shown in Fig. 4b. In these experiments, the maximum current density loss was about 20 % and the loss in the maximum power density $\sim$15 % with 5.6 % CO. Primarily, the explanation of the decrease in the fuel cell power output is due to the blocking of active sites and therefore reducing the electrochemically active surface area (ECSA) on the anode catalyst by strongly bound CO adsorbates. The corresponding reaction is described in Eq. (3.1).

$$\mathrm{CO} + \mathrm{Pt}^* \rightarrow \mathrm{CO} - \mathrm{Pt} \tag{3.1}$$

Pt* free Pt sites on the catalyst surface.

Carbon monoxide chemisorbs on the platinum surface and blocks free sites needed for the hydrogen oxidation reaction (HOR), which leads to a smaller turnover frequency in the proton production. With fewer H^+ available for the water production on the cathode side, the cell performance decreases. The relation between the current density and CO coverage (θ_{CO}) was found to be linear [6, 30] and can be described by Eq. (3.2).

$$i_{(\mathrm{CO}+\mathrm{H}_2)}/i_{(\mathrm{H}_2)} = (1 - \theta_{\mathrm{CO}}) \tag{3.2}$$

$i_{\mathrm{CO}+\mathrm{H}_2}]] >$: current density with CO in the anode feed; i_{H_2}: current density with pure hydrogen at the anode; θ_{CO}: surface coverage of platinum catalysts by CO.

The CO coverage (θ_{CO}), on the other hand, seems to be a linear function of the CO concentration in the anode feed described by Li et al. [6], in the case of working temperatures above 120 °C. This linear behavior was also found in our measurements. At 160 °C and 0.1 V cell voltage, the $i_{\mathrm{CO}+\mathrm{H}_2}/i_{\mathrm{H}_2}$ ratio is a linear function of the CO concentration with a slope of -0.0024 per % CO and a coefficient of determination of $R^2 = 0.9924$ which shows a good agreement of linearity.

Additional to the CO coverage calculation provided by Eq. (3.2), with our reference assembly, we were able to investigate the influence of the CO concentration on the anode overpotential. Therefore, all measured anode

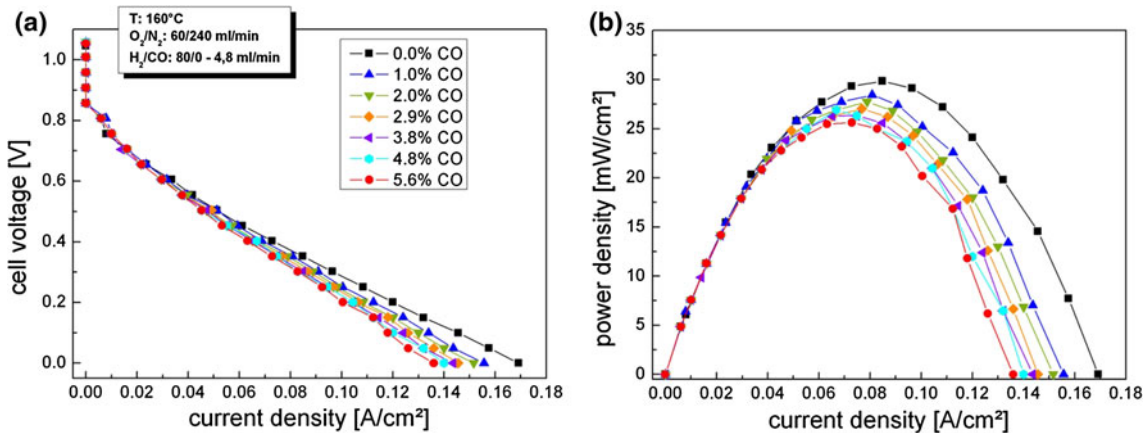

Fig. 4 **a** iV curves with increasing amount of CO in the anode feed. **b** Corresponding power density versus current density curve

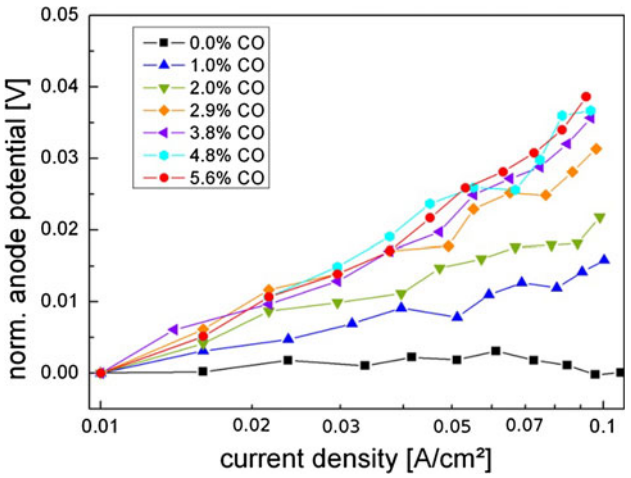

Fig. 5 Normalized anode overpotentials over lg current density with changing CO concentrations. With increasing amount of CO, the anode overpotential slope also increases

Table 1 Anode and cathode potential at 0.1 V cell voltage and the corresponding overpotential slopes between 0.01 and 0.1 A/cm^2 current density

CO conc. [vol. %]	$\Phi_A = \eta_{A\ @\ 0.1\ V}$ (mV)	$\eta_{C\ @\ 0.1\ V}$ (mV)	$\Phi_{C\ @\ 0.1\ V}$ (mV)	$m\ (\eta_A)$ (mV/dec)	$m\ (\eta_C)$ (mV/dec)
0.0	47	189	757	–	–
1.0	55	188	770	15	7
2.0	69	198	761	20	10
2.9	87	212	746	31	16
3.8	92	215	741	35	23
4.8	101	221	737	37	24
5.6[a]	86	203	751	39	22

The slope of the cathode overpotential $m\ (\eta_C)$ was corrected by the 0 % CO slope

[a] Some errors occurred during measurement, so that no reliable values were obtained

potentials were normalized in two steps. In the first step, all measurements were resistance corrected according to the procedure described in the experimental Sect. 2.2. The estimated resistance for the measurement without CO was 39.0 ± 4 mΩ and used for all measurements under the assumption that CO in the anode feed has no influence on the membrane resistance. To show the effect of CO concentration on the anode overpotential, all resistance-corrected measurements were shifted to zero potential at 0.01 A/cm^2 (normalization). The normalized anode overpotentials versus lg current density at different CO concentrations are shown in Fig. 5. By analyzing the slope of η_A between current densities of 0.01 and 0.1 A/cm^2, an increase from 9 mV/dec with 0.0 % CO to 40 mV/dec with 5.6 % CO was found. Beyond the analyzed slopes of the anode overpotentials, the electrode potentials/overpotentials at 0.1 V cell voltage (not normalized) at different CO concentrations are given in Table 1. As expected, an increase in the anode potential with increasing CO concentration at high current densities (low cell voltage, respectively) from ∼50 mV at 0 % CO to ∼100 mV at > 5 % CO is observed. Comparing the anode overpotentials in the analyzed current density region (0.1 A/cm^2), with the reported potentials of phosphoric acid adsorption [14, 17], only negligible H_3PO_4 adsorption on the anode catalyst seems to be possible even with hydrogen containing > 5 % CO.

In addition to the anode potential/overpotential, the η_C and Φ_C as well as the slope of the cathode overpotential induced by the CO contamination of the anode are given in Table 1. The slope of the cathode overpotential was normalized by the cathode slope with 0 % CO to suppress the ORR losses and only shows the relation between the CO concentration and η_C. Surprisingly, the cathode is also affected by CO adsorption on the anode. This can be seen in the increasing value of the cathode overpotential as well as an increase in the cathode overpotential slope with more CO in the anode feed. Therefore, we conclude that the cell voltage loss with increasing amount of CO is not only due to the increase in the anode overpotential, but also the superposition of anode and cathode overpotential. For a clearer demonstration of the effect, in Fig. 6, the anode and cathode potentials versus current density for 0.0 and 5.6 % CO are shown. The increase in η_C can be explained by the reduced "crossover" of protons through the membrane and thus a decreased consumption to form water. This result shows that anode and cathode processes are connected by the proton transfer step. Therefore, they cannot be discussed independently of each other. This cross talk between anode and cathode has been observed before in direct methanol fuel cells reported by Dixon et al. [31]. There, also the influence of a reduced anode ECSA on the cathode potential (catalyst adsorbates, respectively) was observed.

3.3 Synergetic effect of CO and water in the anode fuel

If hydrogen from a reformer is used as feed, not only CO and H_2 reach the fuel cell anode, but also water and CO_2 (carbon dioxide) from the reforming process may enter the fuel cell. Beyond the dilution effect of CO_2 which lowers the hydrogen partial pressure on the anode, it is also possible that small amounts of CO (∼1 % [6]) can be formed by the reversed water gas shift reaction directly on the anode catalyst. The focus of our experiments was the investigation of a possible cleaning of the surface due to the CO electro-oxidation reaction, which is assumed to take place at the applied fuel cell temperature. Therefore, the anode was fed with a gas mixture of H_2, CO and water mimicking the reformate gas without CO_2.

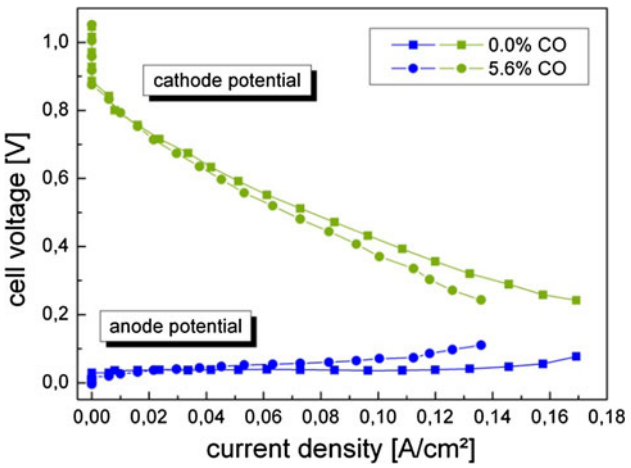

Fig. 6 Comparison of the anode and cathode potential over current density with 5.6 and 0.0 % CO in the fuel gas

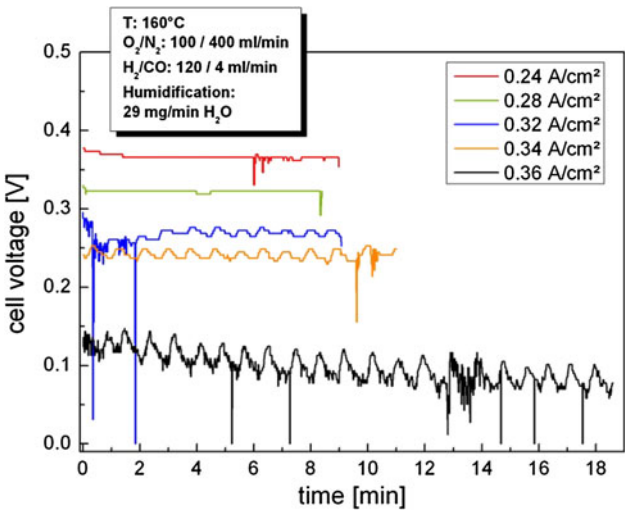

Fig. 7 Cell voltage over time at different constant current densities. Cathode: $O_2/N_2 = 100/400$ ml/min; anode: $H_2/CO = 120/4$ ml/min ($\sim$3.2 % CO). The amount of water introduced by the humidifier was $\sim$29 mg/min

The first results of these investigations are shown in Fig. 7, where different cell voltages corresponding to different current densities are plotted over time. With $\lambda_{H_2} = 1.6$ and $\lambda_{air} = 2.65$, to the maximum current density (0.4 A/cm^2), respectively, effects from fuel starvation can be excluded. The absolute humidity was held constant for all measurements at $\sim$29 mg H_2O/min. With current densities < 0.32 A/cm^2, the cell voltages are constant with time. At higher current densities (i.e., cell voltages < 300 mV), the cell voltage starts to oscillate. In additional measurements with only CO or only water in the anode fuel, no oscillations were observed. Therefore, an influence from the humidifier or the heating elements (periodic heating times, etc.) can be excluded, and the

Table 2 Wave parameters of the oscillations at different current densities

Current density (A/cm^2)	Half wavelength (s)	Peak-to-peak amplitude (mV)
0.24	–	0
0.28	–	0
0.32	25	7.8
0.34	26	12.8
0.36	24	33.3

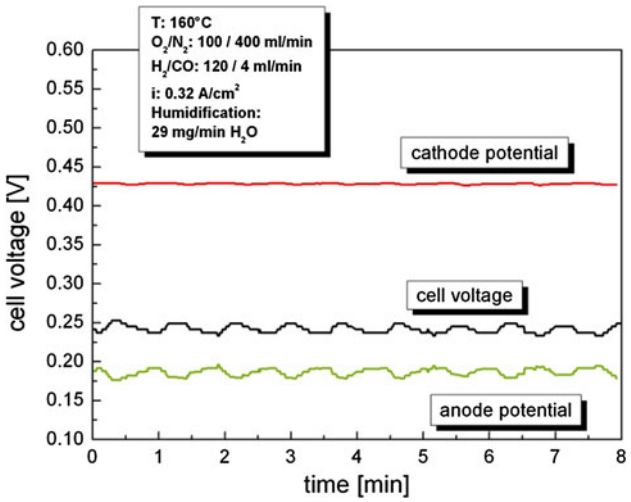

Fig. 8 Cell voltage and electrode potentials at 0.32 A/cm^2. The CO concentration in the anode fuel gas was about 3.2 %. The amount of water introduced by the humidifier was $\sim$29 mg/min. While the cathode potential remains constant over time, the anode potential oscillates

observed effect can be related to electrode reactions. With an increase in current density, the amplitude of the oscillations increases, while the period stays constant. An overview of the measured parameters is given in Table 2. The maximum peak-to-peak amplitude of $\sim$33 mV was observed at 0.36 A/cm^2 while the half wavelength for all observed oscillations was around 25 s. To investigate the origin of the occurring oscillations, Fig. 8 shows the variation of Φ_C, Φ_A and the cell voltage with time at 0.32 A/cm^2. By measuring the anode and cathode potentials separately (Fig. 8), the assumption that the cell voltage oscillation is due to the oscillating anode overpotential can be confirmed. While the anode potential shows the mirrored cell voltage potentials, the cathode potential, in contrast, is almost stable and shows amplitudes of only about $\pm$ 1 mV at current densities of 0.32 A/cm^2.

The mechanisms and extent of the anode humidification become important, when we assume, that CO poisoning is a reversible process at HT-PEM working temperatures. Possible reactions to reduce the CO fraction in the anode

gas are the water gas shift reaction (3.3) and the electro-oxidation of CO on the Pt surface (3.4).

$$CO + H_2O \leftrightarrow CO_2 + H_2 \quad (3.3)$$

$$CO - Pt + OH - Pt \rightarrow CO_2 \uparrow + 2Pt^* + 2H^+ + 2e^- \quad (3.4)$$

As the water gas shift reaction shows very slow kinetics below 200 °C [32], it can be neglected. However, an indication that reaction (3.4) occurs in the working HT-PEM fuel cell is the occurrence of oscillations in the cell voltage. Oscillations due to the CO electro-oxidation reaction (3.4) have been observed in electrochemical half-cell measurements [33–35], low-temperature PEM fuel cell investigations [36, 37] and hydrogen pumping experiments [38, 39] before. But all of these investigations have been performed at 25 °C or only slightly elevated temperatures. The explanation for their appearance is the increase in the anode potential up to the point, when OH from the water activation (3.5) can adsorb on the catalyst surface.

$$H_2O + Pt^* \rightarrow OH - Pt + H^+ + e^- \quad (3.5)$$

At this point, CO reacts with the adsorbed OH (3.4) and leaves the surface. Thus, cleaning the surface from CO, the anode potential decreases again and hydroxide adsorption ceases. With no OH on the surface, a stable CO coverage is recovered and the overpotential increase starts again.

However, it is also known that water dissociation (3.5) starts at potentials around 0.6 V as found by XPS [40] and during hydrogen pumping experiments investigating the ethanol oxidation reaction at room temperature [41]. We propose that the onset potential of water dissociation is not much lower at 160 °C. But the measured anode potential does not exceed 0.2 V. Therefore, we suppose that additional reactions on the anode influence the oscillation behavior. Parameters not mentioned yet are the influence of the hydrogen oxidation reaction and anion adsorption, which can start at the measured anode potentials. Both are reported to have an effect on the oscillation behavior. Malkhandi et al. [34, 35] described an influence of anion (Cl^- and Br^-) adsorption processes on the occurring oscillations measured in an electrochemical cell assembly. But the fact, that the parameters (temperature, electrolyte, etc.) they used are far from our fuel cell experiment conditions, makes a comparison complicated. Adopting their observations for HT-PEM fuel cells, phosphoric acid anions could play a similar role in the oscillation behavior. H_3PO_4 could possibly be a mediator in the CO oxidation, as it is known that although its maximum adsorption coverage is around 0.6–0.8 V, the reduction in phosphoric acid on Pt surfaces starts earlier at elevated temperatures.

A second factor is the hydrogen oxidation reaction and the resulting current. Its influence on the voltage oscillations was modeled by Siegmeier et al. [42] for low-temperature PEM fuel cells. The presence of the hydrogen oxidation reaction on the catalyst surface forces the oscillation wavelength into the same timescale (seconds) as we measured with our HT-PEM experiments (Table 2). The reported potential where CO electro-oxidation starts in their model is about 0.7 V and thus can also not explain our investigations. To clarify the nature of the oscillation behavior in phosphoric acid HT-PEM fuel cells, further experiments determining the adsorbate coverage of the catalyst have to be performed.

An additional observation of these experiments is that the CO electro-oxidation only occurred with an external humidification of the anode. Experiments with no humidification on the anode did not show oscillations in the cell voltage, even at high current densities. Therefore, the amount of water from the cathode entering the anode, which can be up to 20 % in cases of a dry anode, seems to be too low to start the effect.

4 Summary and conclusions

Recently, it was possible to integrate a reference electrode into a conventional HT-PEM fuel cell setup, so that we were able to record the anode and cathode potential separately and reliably. It is the first time that results of a HT-PEM fuel cell with this kind of reference electrode are reported.

In operation with pure hydrogen on the anode and synthetic air on the cathode, the anode overpotential shows only a small increase even at higher cell currents. The cathode potential therefore decreases as fast as the cell voltage at low current densities. At higher current densities, the difference between the i–V curve and the cathode potential is due to the membrane resistance. In this operation mode, potential-dependent phosphoric acid adsorption and poisoning on the fuel cell cathode due to blocking of active sites is held responsible for the reduced fuel cell performance. Due to the low anode overpotential, no limiting effects from phosphoric acid adsorption at the anode are expected.

By dosing different CO concentrations in the anode fuel, not only the slope of the anode overpotential increased with the CO amount, but also the cathode overpotential. This was explained by the cross talk between the electrodes. By blocking the surface for the HOR, fewer protons were produced. This also affects the ORR on the cathode. With fewer protons undergoing the water production on the cathode, the overpotential on this side also increases. The resulting loss in fuel cell performance is therefore explained by the reduction in ECSA at the anode and an increase in both anode and cathode overpotential.

Another HT-PEM fuel cell effect investigated was voltage oscillations by adding CO and water to the anode fuel at high constant current densities. With the reference electrode assembly, it was possible to show that these oscillations are related to processes at the anode side and have only little influence on the cathode overpotential. The ad- and desorbing mechanisms on the catalyst surface, which lead to this behavior, have not been explained yet. The cleaning of the catalyst surface by the oxidation of CO through adsorbed OH seems to be the main cause of the oscillations. But the fact, that OH starts to adsorb on Pt surfaces at potentials lower than 0.6 V and that the anode overpotential cannot reach these, suggests different or additional effects from other adsorbates (like H_3PO_4) for an explanation. So further measurements like in situ XAS, XPS or in situ DRIFTS should be used to clarify the adsorbate coverage with time during the oscillations to gain deeper insight into this mechanism.

Acknowledgments The authors thank Dr. Maria Daletou from Advent (Greece) and Dr. Tomáš Klicpera from Fumatech (Germany) for the preparation of the MEAs. Dr. Dietmar Gerteisen (Fraunhofer ISE, Freiburg, Germany) is gratefully acknowledged for the helpful discussions as well as Sebastian Lang (TU Darmstadt) for his experienced PBI production. Financial support for this effort was provided by the EU project DEMMEA, Seventh Framework Programme.

References

1. Behling NH (2013) History of phosphoric acid fuel cells. In: Current technology challenges and future research needs, 1st edn. Elsevier, Amsterdam, pp 53–134
2. Hart D, Hörmandinger G (1998) Environmental benefits of transport and stationary fuel cells. J Power Sources 71:348–353
3. Larminie J, Dicks A (2003) Medium and high temperature fuel cells. In: fuel cell systems explained, 2nd edn. John Wiley & Sons Ltd., Weinheim, pp 163–187
4. Wainright JS, Wang J-T, Weng D, Savinell RF, Litt M (1995) Acid-doped polybenzimidazoles: a new polymer electrolyte. J Electrochem Soc 142:L121–L123
5. Li Q, Jensen JO, Savinell RF, Bjerrum NJ (2009) High temperature proton exchange membranes based on polybenzimidazoles for fuel cells. Prog Polym Sci 34(5):449–477
6. Li Q, He R, Gao J-A, Jensen JO, Bjerrum NJ (2003) The CO poisoning effect in PEMFCs operational at temperatures up to 200 °C. J Electrochem Soc 150:A1599–A1605
7. Zhang J, Xie Z, Zhang J, Tang Y, Song C, Navessin T, Shi Z, Song D, Wang H, Wilkinson DP, Liu Z-S, Holdcroft S (2006) High temperature PEM fuel cells. J Power Sources 160(2):872–891
8. Schmidt TJ, Baurmeister J (2008) Properties of high-temperature PEFC Celtec®-P 1000 MEAs in start/stop operation mode. J Power Sources 176(2):428–434
9. Hansen JB (2003) Methanol reformer design considerations. In: Vielstich W, Gasteiger HA, Lamm A (eds) Handbook of fuel cells, vol. 3 fuel cell technology and applications. Wiley, Weinheim, pp 141–148
10. Larminie J, Dicks A (2003) Fuelling fuel cells. In: Fuel cell systems explained, 2nd edn. Wiley, Weinheim, pp 229–307
11. Sugishima N, Hinatsu JT, Foulkes FR (1994) Phosphorous acid impurities in phosphoric acid fuel cell electrolytes. J Electrochem Soc 141(12):3325–3331
12. Ye S, Kita H, Aramata A (1992) Hydrogen and anion adsorption at platinum single crystal electrodes in phosphate solutions over a wide range of pH. J Electroanal Chem 333(1–2):299–312
13. He Q, Yang X, Chen W, Mukerjee S, Koel B, Chen S (2010) Influence of phosphate anion adsorption on the kinetics of oxygen electroreduction on low index Pt(hkl) single crystals. Phys Chem Chem Phys 12(39):12544–12554
14. Zelenay P, Scharifker BR, Gervasio D, Bockris JO′M (1986) A comparison of the properties of CF_3SO_3H and H_3PO_4 in relation to fuel cells. J Electrochem Soc 133(11):2262–2267
15. Weber M, Nart FC, Moraes IR, Iwasita T (1996) Adsorption of phosphate species on Pt(111) and Pt(100) as studied by in situ FTIR spectroscopy. J Phys Chem 100(51):19933–19938
16. Santos MC, Miwa DW, Machado SAS (2000) Study of anion adsorption on polycrystalline Pt by electrochemical quartz crystal microbalance. Electrochem Commun 2:692–696
17. He Q, Shyam B, Ramaker D, Mukerjee S (2013) Mitigating phosphate anion poisoning of cathodic Pt/C catalysts in phosphoric acid fuel cells. J Phys Chem C 117(10):4877–4887
18. Büchi FN, Scherer GG (2001) Investigation of the transversal water profile in Nafion membranes in polymer electrolyte fuel cells. J Electrochem Soc 148(3):A183
19. Kuhn H, Andreaus B, Wokaun A, Scherer GG (2006) Electrochemical impedance spectroscopy applied to polymer electrolyte fuel cells with a pseudo reference electrode arrangement. Electrochim Acta 51(8–9):1622–1628
20. Mitsuda K, Murahashi T (1991) Air and fuel starvation of phosphoric acid fuel cells: a study using a single cell with multi-reference electrodes. J Appl Electrochem 21(6):524–530
21. Adler SB, Henderson BT, Wilson MA, Taylor DM, Richards RE (2000) Reference electrode placement and seals in electrochemical oxygen generators. Solid State Ionics 134:35–42
22. Li G, Pickup PG (2004) Measurement of single electrode potentials and impedances in hydrogen and direct methanol PEM fuel cells. Electrochim Acta 49(24):4119–4126
23. Siroma Z, Kakitsubo R, Fujiwara N, Ioroi T, Yamazaki S-I, Yasuda K (2006) Compact dynamic hydrogen electrode unit as a reference electrode for PEMFCs. J Power Sources 156(2):284–287
24. Li G, Pickup PG (2006) Analysis of performance losses of direct ethanol fuel cells with the aid of a reference electrode. J Power Sources 161(1):256–263
25. Liu Z, Wainright J, Huang W, Savinell RF (2004) Positioning the reference electrode in proton exchange membrane fuel cells: calculations of primary and secondary current distribution. Electrochim Acta 49(6):923–935
26. He W, Nguyen TV (2004) Edge effects on reference electrode measurements in PEM fuel cells. J Electrochem Soc 151(2): A185–A195
27. Hinds G, Brightman E (2012) In situ mapping of electrode potential in a PEM fuel cell. Electrochem Commun 17:26–29
28. Heinzel A, Bandlamudi G, Lehnert W (2009) Fuel cells—proton-exchange membrane fuel cells | high temperature PEMFCs: 951–957
29. Daletou MK, Kallitsis JK, Voyiatzis G, Neophytides SG (2009) The interaction of water vapors with H_3PO_4 imbibed electrolyte based on PBI/polysulfone copolymer blends. J Membr Sci 326(1):76–83
30. Igarashi H, Fujino T, Watanabe M (1995) Hydrogen electro-oxidation on platinum catalysts in the presence of trace carbon monoxide. J Electroanal Chem 391(1–2):119–123
31. Dixon D, Habereder A, Farmand M, Kaserer S, Roth C, Ramaker DE (2012) Space resolved, in Operando X-ray absorption spectroscopy: investigations on both the anode and cathode in a direct methanol fuel cell. J Phys Chem C 116(13):7587–7595
32. Bergmann A, Gerteisen D, Kurz T (2010) Modelling of CO poisoning and its dynamics in HTPEM fuel cells. Fuel Cells 10(2):278–287

33. Schmidt TJ, Grgur B, Markovic N, Ross PN (2001) Oscillatory behavior in the electrochemical oxidation of formic acid on Pt(100): rotation and temperature effects. J Electroanal Chem 500(1–2):36–43
34. Malkhandi S, Bonnefont A, Krischer K (2009) Dynamic instabilities during the continuous electro-oxidation of CO on poly- and single crystalline Pt electrodes. Surf Sci 603(10–12):1646–1651
35. Malkhandi S, Bauer P, Bonnefont A, Krischer K (2013) Mechanistic aspects of oscillations during CO electrooxidation on Pt in the presence of anions: experiments and simulations. Catal Today 202:144–153
36. Rohland B, Plzak V (1999) The PEMFC-integrated CO oxidation—a novel method of simplifying the fuel cell plant. J Power Sources 84:183–186
37. Smolinka T (2005) Untersuchungen an einer mit Reformat betriebenen PEM-Brennstoffzelle. Dissertation, University of Ulm, Germany
38. Farrell C, Gardner C, Ternan M (2007) Experimental and modelling studies of CO poisoning in PEM fuel cells. J Power Sources 171(2):282–293
39. Kadyk T, Kirsch S, Hanke-Rauschenbach R, Sundmacher K (2011) Autonomous potential oscillations at the Pt anode of a polymer electrolyte membrane fuel cell under CO poisoning. Electrochim Acta 56(28):10593–10602
40. Wakisaka M, Suzuki H, Mitsui S, Uchida H, Watanabe M (2009) Identification and quantification of oxygen species adsorbed on Pt(111) single-crystal and polycrystalline Pt electrodes by photoelectron spectroscopy. Langmuir 25(4):1897–1900
41. Melke J, Schoekel A, Gerteisen D, Dixon D, Ettingshausen F, Cremers C, Roth C, Ramaker DE (2012) Electrooxidation of ethanol on Pt. An in Situ and time-resolved XANES study. J Phys Chem C 116(4):2838–2849
42. Siegmeier J, Baba N, Krischer K (2007) Bistability and oscillations during electrooxidation of H2-CO mixtures on Pt: modeling and bifurcation analysis. J Phys Chem C 111(36):13481–13489